LAWRENCE
LIVERMORE
NATIONAL
LABORATORY

UCRL-PROC-231439

Electrons in a Positive-Ion Beam with Solenoid or Quadrupole Magnet Transport

A. W. Molvik, R. H. Cohen, A. Friedman, M. Kireeff Covo, S. M. Lund, W. M. Sharp, P. A. Seidl, F. M. Bieniosek, J. E. Coleman, A. Faltens, P. K. Roy, J. L. Vay, L. Prost

June 4, 2007

International Workshop on Electron Cloud Effects - Ecloud'07
Deagu, South Korea
April 9, 2007 through April 12, 2007

ELECTRONS IN A POSITIVE-ION BEAM WITH SOLENOID OR QUADRUPOLE MAGNETIC TRANSPORT

A. W. Molvik[#], R. H. Cohen, A. Friedman, M. Kireeff Covo, S. M. Lund, W. M. Sharp, Heavy Ion Fusion Science Virtual National Laboratory, Lawrence Livermore National Laboratory, Livermore, CA 94550, USA.

P.A. Seidl, F. M. Bieniosek, J.E. Coleman, A. Faltens, P.K. Roy, J.L. Vay, Heavy Ion Fusion Science Virtual National Laboratory, Lawrence Berkeley National Laboratory, Berkeley, CA 94720, USA.

L. Prost, FermiLab, Batavia, IL 60510-0500, USA

Abstract

The High Current Experiment (HCX) is used to study beam transport and accumulation of electrons in quadrupole magnets and the Neutralized Drift-Compression Experiment (NDCX) to study beam transport through and accumulation of electrons in magnetic solenoids. We find that both clearing and suppressor electrodes perform as intended, enabling electron cloud densities to be minimized. Then, the measured beam envelopes in both quadrupoles and solenoids agree with simulations, indicating that theoretical beam current transport limits are reliable, in the absence of electrons. At the other extreme, reversing electrode biases with the solenoid transport effectively traps electrons; or, in quadrupole magnets, grounding the suppressor electrode allows electron emission from the end wall to flood the beam, in both cases producing significant degradation in the beam.

INTRODUCTION

Electron cloud effects (ECEs) [1] and beam-induced pressure rises [2], that are frequently observed to limit the performance of high-energy physics colliders and high-intensity rings, are also a concern for future high-intensity heavy-ion linear accelerators such as envisioned in Heavy Ion Inertial Fusion (HIF) [3] and as applied in the near term to high-energy-density physics (HEDP) [4,5]. We are engaged in an experimental and theoretical program to measure, understand, and model these effects in heavy-ion accelerators [6-20].

In this paper, we report the use of clearing electrodes to remove electrons from the drift regions between quadrupole or solenoid magnets and also to measure the electron flow; a suppressor electrode to block (or allow) the flow of electrons from the end wall; an electrode in the center of each solenoid that can be biased negatively to expel electrons; and an electrode, lining the beam tube in the last quadrupole magnet, that serves as a capacitive electrode in addition to measuring electron emission and collection.

Clearing electrodes have been successfully used in conjunction with stripper-foil biasing and electron bending magnets to remove several classes of electrons that were generated at the stripping foil in the Proton Storage Ring (PSR) injection region [21]. Clearing electrodes have also been used to remove ions from negatively charged beams (electrons or antiprotons) [22-29]. In some experiments, the maximum stored electron current increased by factors of up to 6 [26,28]. Different electrode configurations have been successfully used: dipole electric fields from long partial cylinders on opposite sides of the ion beam [21], button probes flush with walls for low coupling impedance with the stored electron beam [23,24,28], and strip lines [26,28]. Button probes are frequently used in drift regions or in negative potential well pockets formed by enlargements of the chamber [22], with strip lines along the length or at both ends of bending magnets [22,28] or also in straight sections [26].

On the High Current Experiment (HCX), we chose a different clearing electrode configuration — we use a ring electrode surrounding the beam in each drift region between quadrupole magnets, with a positive bias to attract electrons, as will be described in more detail in the next section. The HCX provides a 1 MeV, 180 mA, K+ ion beam that has been used to study ion beam transport in electrostatic quadrupoles [30], beam induced electron emission and gas desorption [7,12,17], and electron cloud and gas effects in magnetic quadrupoles with a field gradient of ~10 T/m. The beam has a space-charge potential of ~2 kV, a rise time of 0.4 μs and fall time of 1 μs, a flattop duration of 4 μs, and a pulse repetition interval of 10 s. An aperture can be inserted at the D2 diagnostic region, immediately preceding the magnetic quadrupoles, to reduce the beam current to 32 mA and ~300 V beam potential. Electron transit times between walls are in the range of 4 ns (11 ns if apertured) for an unneutralized beam, almost 3 orders of magnitude shorter than the flattop duration. This enables exploration of unique electron trapping regimes: beam-induced multipactor trapping, that is frequently observed with in rf accelerators, will not occur during the flattop, and trailing edge multipactor is not an issue because any electrons generated will be lost before the next pulse in ~10 s. However electrons, emitted from a beam-tube wall under beam bombardment, will be trapped during the current rise at the beam head. Ionization of gas by the beam generates electrons that are deeply trapped; the associated ions from gas are expelled in ≤1 μs. Electrons, emitted

[#]awmolvik@lbl.gov

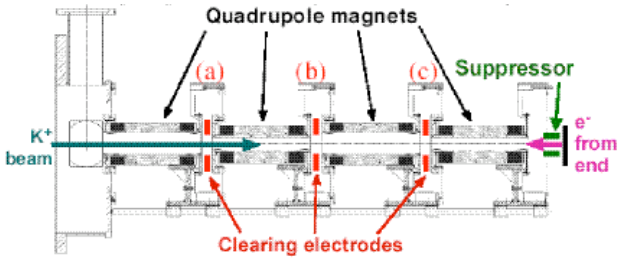

Figure 1. Magnetic quadrupole region of HCX, from D2 diagnostic region on the left to the D-End diagnostic region beginning on the right. The half lattice length is 0.52 m. Clearing electrodes a, b, and c are shown in the drift regions between each pair of quadrupoles. A suppressor electrode prevents beam induced electron emission, from structures hit by beam in D-End, from reaching the quadrupole magnets.

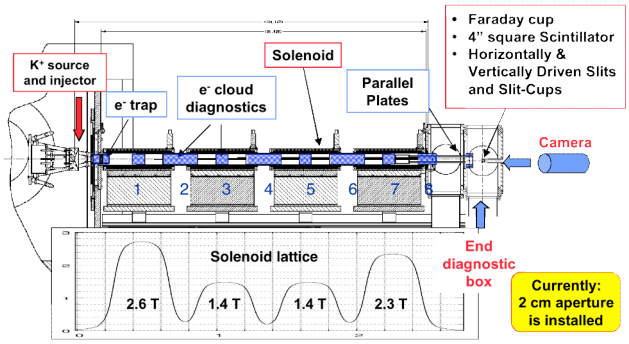

Figure 2. Four solenoid magnets assembled on the solenoid transport section of the NDCX. The e-cloud diagnostics are shown in blue, labeled with their numbers. The peak magnetic fields are listed for each magnet for the operating beam envelope.

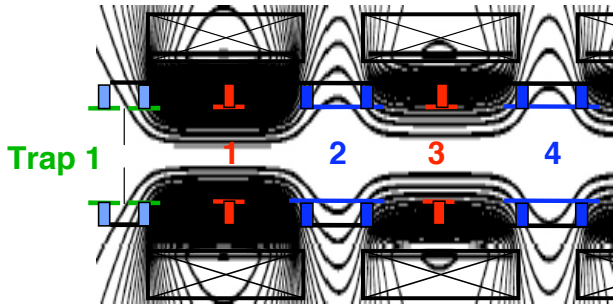

Figure 3. Expanded view of first 2.2 solenoids of NDCX, showing e-cloud electrodes relative to the magnetic field. Magnetic field lines map from the downstream electrode of e-trap 1, to e-cloud electrode 2, and extend from the wall into the outer half of the beam radius.

from an end wall, will be pulled into the positive beam potential, and will be transported upstream in quadrupole magnets by electron drifts (E×B, grad-B, and curvature). Suppression and clearing of these backstreaming electrons, or consequences for the beam if electrons accumulate, is the subject of this paper.

On the Neutralized Drift-Compression Experiment (NDCX) we carried out experiments to study the matching and transport of a space-charge-dominated ion beam in the solenoid transport channel, paying particular attention to the effects of gas and electrons on the beam. The nominal energy of the potassium (K+) beam was 300 keV, and the beam current, limited by a 1-cm-radius aperture, was in the range of 26-30 mA for all the data shown here. This facility has demonstrated longitudinal beam compression by a factor of 50 [31]. The e-cloud experiments will be described in greater detail elsewhere [32]. Here we discuss some highlights. The setup for these four-solenoid-transport experiments is shown in Fig. 2.

Solenoid midpoints are separated by 60 cm, and the beam-pipe inner radius is 4.6 cm. Gaps were provided between solenoids to allow for acceleration or diagnostics on future facilities. The magnetic field decreases by factors of several in these gaps, resulting in some magnetic field lines intercepting the beam pipe; this is quite different from using solenoidal fields to suppress electron clouds, for which a uniform strength field is desired so that electrons from the wall cannot reach the beam [33]. Beam diagnostics are provided in an end tank, as shown in Fig. 2. The beam at the exit of the diode was also characterized in detail with identical diagnostics for all runs. A set of electron-cloud diagnostics was installed and commissioned.

These "e-cloud" diagnostics consist of short (8.5 cm long) cylindrical electrodes in the center of each solenoid magnet, and long (25 cm long) cylindrical electrodes covering the gaps between magnets to intercept expanding magnetic flux [16]. We will refer to these as "solenoid electrodes" and "gap electrodes" respectively, and we label them E1 through E7. These electrode can be independently biased between ±1 kV. In particular, the solenoid electrodes can be biased negatively to repel electrons, while the gap electrodes can be biased positively to clear electrons from intercepted field lines and suppress emission. Reversing the biases, we can trap electrons that are emitted from the gap electrodes between magnets. Electrodes E1 through E7, shown in Fig. 3, measure and control electrons on the outer flux tubes through the beam. An added electrode E8, originally called Trap 2, intercepts flux through the inner radii of the beam to within 0.75 cm of the axis, providing additional control of electrons on the inner flux tubes. The functions of the suppressor electrode on HCX are filled by E8 and by a pair of parallel plates near the end-wall, which can be biased to collect either ions or electrons.

The electrostatic particle-in-cell code WARP [34,35] has been upgraded to handle multiple species and to model such species interactions as gas desorption, collisional ionization, and release of electrons from walls [20]. Primary and secondary electron production at walls is managed by the POSINST electron-cloud package [36], while impact ionization is handled by the txPhysics library [36]. An additional module handles desorption of neutrals [9]. Electrons are advanced with a time step that is one fifth that of heavier species, and a "drift-Lorentz" electron-advance algorithm [11] allows time steps much

greater than their gyrofrequency. In addition, the Chombo mesh-refinement code [8] is incorporated into WARP but is used only where noted in the simulations reported here.

TESTS OF SUPPRESSOR AND CLEARING ELECTRODES

These electrodes were tested first with quadrupole beam transport; secondly, a revised set was tested with solenoid beam transport.

Quadrupole transport

Fig. 1 shows the HCX in the region of four magnetic quadrupoles. To the left is the D2 diagnostic region (preceded by 10 electrostatic quadrupoles) followed by 4 magnetic quadrupoles. Each magnetic quadrupole has 30 cm long magnetic field coils in a 47 cm length elliptical tube that has minor and major inner radii of 3 cm and 5 cm respectively. Seven ports provide diagnostic access in the 5 cm gap between each pair of magnets, and after the last one.

A suppressor ring, that is 10 cm diameter and 10 cm long, was installed surrounding the beam after it exits the last magnet. It can be biased to –10 kV to prevent electrons that are created by beam impinging on metal surfaces from being transported back into the quadrupole magnets. For these experiments, the front plate of a slit scanner is inserted, providing a grounded-metal end-wall surface on which the ion beam impinges, generating ≥6 electrons per incident ion [7]. It is located about 30 cm downstream of the end of the last quadrupole magnet winding.

Clearing electrodes were installed in the 5 cm gaps between quadrupole magnets for the purpose of sweeping electrons from each drift region by applying a positive bias voltage. Each clearing electrode is a circular ring, concentric with the beamline axis with a toroidal inner diameter of 8 cm and a poloidal diameter of 1.3 cm. This places the electrodes ~1 cm outside of the magnet bore so that beam halo ions do not strike them.

A capacitive electrode, 28 cm long, surrounding the beam and nearly flush to the 3 x 5 cm radius magnet bore was installed in the fourth magnetic quadrupole.

The currents to the capacitive electrode in the fourth magnet and to each of three clearing electrode are shown in Fig. 4 with the suppressor electrode biased to 0 and –10 kV, The capacitive electrode shows the expected positive value during the beam head and negative value during the tail, Fig. 4(a), which results from capacitively coupling to the rising beam potential at the head and to the falling potential at the tail of the beam. When the suppressor is biased to –10 kV, we observe during the nearly flat portion of the beam pulse that the capacitive current changes from negative to positive (from collecting to emitting electrons) and the positively biased clearing electrode-c current decreases to about half its previous value, indicating that about half of the electrons originate at the end wall and half elsewhere — precisely where is left to future investigations. These measurements all

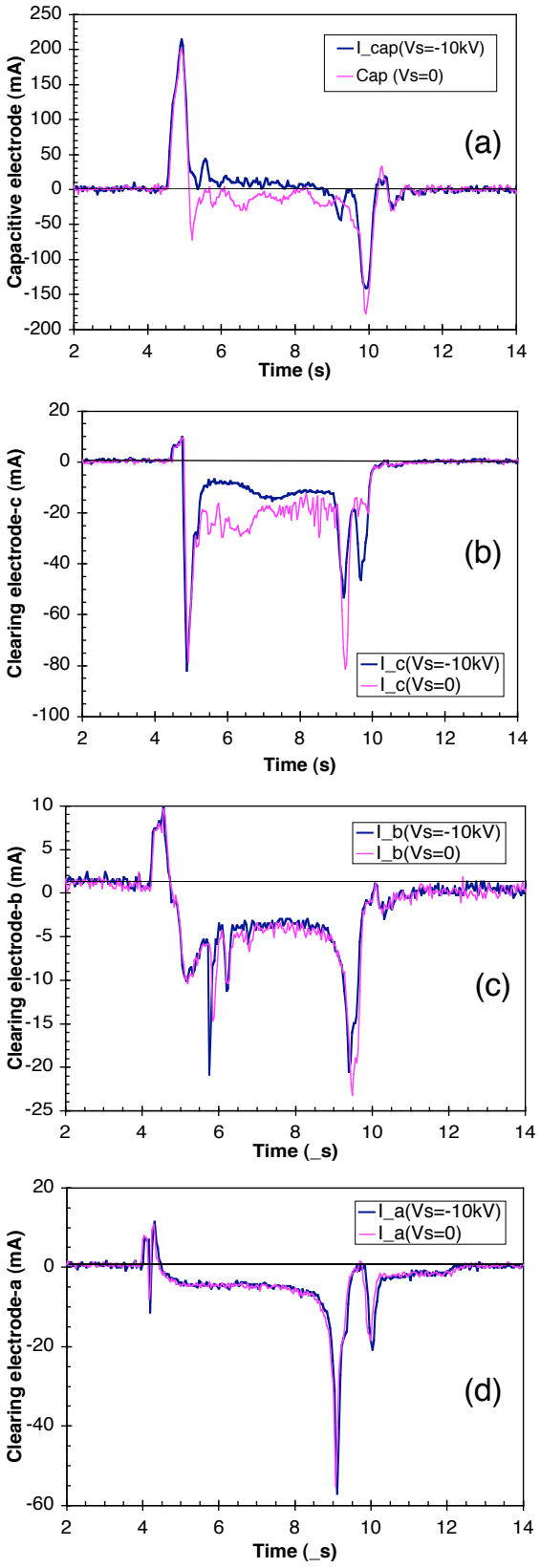

Figure 4. Currents to (a) a capacitive electrode in quadrupole magnet 4, (b) clearing electrode-c between magnets 3 and 4, (c) clearing electrode-b between magnets 2 and 3, and (d) clearing electrode-a between magnets 1 and 2 (See Fig. 1 for locations).

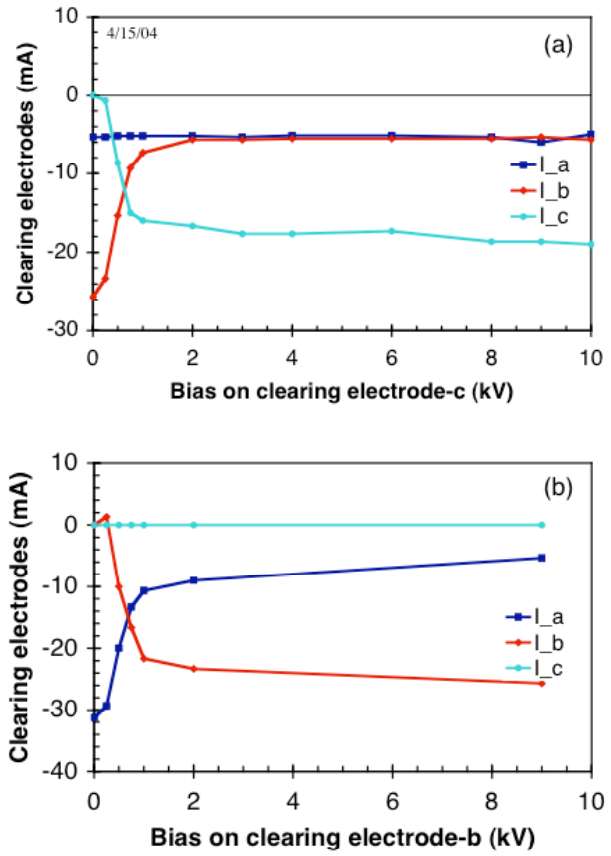

Figure 5. (a) The bias on clearing electrode (c) is varied, with electrodes (a) and (b) biased to +9 kV, and the suppressor electrode at 0 V. (b) The bias on clearing electrode (b) is varied, with electrode (c) at 0, and (a) is at +9 kV.

indicate fewer electrons in the quadrupole magnets when the suppressor is biased to –10 kV. This, combined with voltage scans showing similar currents for all suppressor biases greater than-5 kV, is consistent with the suppressor blocking electron flow from the end wall when biased to –10 kV.

As mentioned, the current to clearing electrode-c (between the third and fourth quadrupole magnets) is also strongly affected by the suppressor electrode, decreasing by about a factor of two when the suppressor is on at –10 kV, Fig. 4(b). This demonstrates that electrons drift upstream through the fourth quadrupole magnet to reach clearing electrode-c. However, the currents to clearing electrode-a and electrode-b are unaffected by the suppressor bias, the currents are nearly identical to electrode-b and even more identical to electrode-a, Fig. 4(c,d). To better quantify how identical the currents are, we average the difference in the currents between 7 and 8.5 μs, finding that the change in current to electrode-a is 0.2±0.6 mA, while that to electrode-b is 0.6±0.6 mA, both small compared with the change in current to clearing electrode-c current of ~5-20 mA. This indicates that clearing electrode-c is performing as it was intended to; it removes essentially all electrons from the drift region between magnets 3 and 4.

We further test the operation of the clearing electrodes by leaving the suppressor voltage at zero to allow back-streaming electrons to flow into the magnetic quadrupoles, then measuring the current to each clearing electrode as we vary the potential on one clearing electrode at a time. In Fig. 5(a), we plot the current to each clearing electrode as the potential on clearing electrode-c is varied while the bias voltages on electrodes-a and electrode-b are held constant at +9 kV. Small changes in current are observed for bias voltages between 1 and 4-8 kV. Below +1 kV, the current to electrode-c decreases from –19 mA to zero, while that to electrode-b increases from –5 to –25 mA, and that to electrode-a stays constant at ~-5 mA because any electrons that get past electrode-c are cleared by electrode-b.

In Fig. 5(b), we vary the bias on electrode-b, while the bias of electrode-c is left at zero, the bias of electrode-a is at +9 kV, and the bias of the suppressor is still at zero. The behavior is analogous to that above, the current to electrode-b remains nearly constant for bias voltages exceeding +1 kV, then decreases from –7 mA to zero below 1 kV bias. As the current to electrode-b decreases, that to electrode-a increases by a similar amount, and that to electrode-c remains near zero.

These results all indicate that the clearing electrodes are performing as intended: when biased to a sufficiently high positive voltage, a clearing electrode removes essentially all the electrons in that drift region. For example, if the bias on electrode-c is not high enough, then electrons leak through to electrode-b increasing its current, but electrode-b removes all the electrons from that drift region as intended so that the current to electrode-a remains constant. Similarly, if the bias on electrode-b is lowered, electrons can leak through to electrode-a.

The bias voltage required for effective clearing is less than we expected: most of the effectiveness (~85%) is achieved with a clearing-c bias of +1 kV, with the remaining 15% gain in effectiveness as the bias increases to +4 to 8 kV. First, we expected that injection from the end would fill the entire beam cross section with electrons, including deeply trapped electrons on the beam axis that would require a bias exceeding the beam potential to remove them. Second, for the electrode geometry: 1.3 cm minor diameter, 8 cm major (inner) diameter, we expected to need a considerably higher electrode bias to overcome the beam potential on axis. This may match our expectations for the beam near the axis, the final 15% of current is likely to come from the inner 15% of the beam, which corresponds to the inner 40% of the radius, and this required 2-8 kV to clear from the drift region. In other work, we separately studied the clearing of weakly and deeply trapped electrons [16]. We found that a clearing electrode bias of +300 V was sufficient to remove most weakly trapped electrons and about +1000 V was sufficient to remove most deeply trapped electrons; however the latter value may be low because new weakly-trapped electrons are being generated at the end-of-pulse at the same time that deeply

trapped electrons are detrapped and we cannot distinguish the two populations.

The electron cloud line charge (in Coulomb/m) has been measured to reach 79-89% of the beam line charge when the suppressor electrode bias is zero [13]. Slit scans under these conditions show a severe "Z-shaped" distortion of X-X' phase space, which is reproduced by the WARP code [11]. The electron cloud line charge is minimized to ≤7% when the suppressor and clearing electrodes are all biased to –10 kV and +9 kV respectively [13]. Under these conditions, slit scans in experiment and simulation show little or no distortion of X-X' phase space due to electrons [11]. It is clearly important to limit the influx of electrons, as uncontrolled electron clouds can significantly degrade an ion beam within only two lattice periods. It is encouraging that suppressor electrodes can limit the influx, and clearing electrodes can reduce the electron line charge by factors of at least three [13].

Solenoid Transport

Recent NDCX runs use the four-solenoid layout shown in Fig. 2. WARP simulations show that, in the absence of electrons, the tune indicated in the figure (2.6 T, 1.4 T, 1.4 T, 2.3 T) catches the beam after the 1-cm-radius aperture and maintains a fairly constant 2-cm radius through the lattice, until the final solenoid pinches the beam to 0.8 cm. We normally run the solenoids with the axial component of the magnetic field aligned in the same direction.

Overlaying the measured current to each of the internal electrodes shows several interesting features. The dominant feature shown in Fig. 6(a) is the capacitive pickup from the beam head. We note that the signals are displaced in time, corresponding to the time of flight of the beam to each electrode, corroborating the number and location of electrodes, and the width of the spikes alternates between narrow and wider, corresponding to the short solenoid electrodes and the longer gap electrodes respectively. In addition, the peak amplitude increases at successive electrodes. We attribute this increasing amplitude to drift-compression of the beam head, resulting from the increasing voltage at the head of the Marx waveform. This interpretation is supported by Faraday cup data. No current spike is observed at the beam head immediately after the source, but after two solenoids, we see a leading spike of 30-40 mA, and after four solenoids, the spike has grown to 40-60 mA.

Simulations of the current to each electrode are shown in Fig. 6b. We note that each of the features of the measurements discussed above is also seen here. The time-of-flight displacements, the growth of the signal (although not as pronounced), and the alternating of longer and shorter electrodes are all apparent. The initial magnitude is similar, near 20 mA, but the current in the simulations grows to about 30 mA whereas the Figure 6.

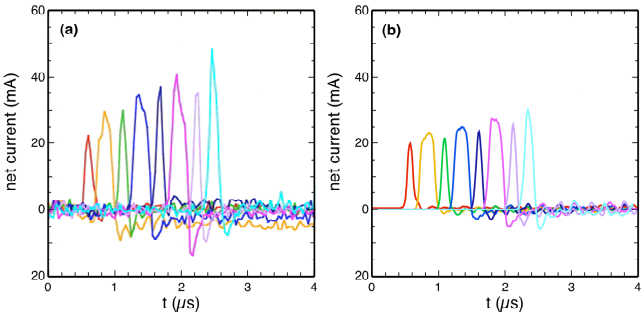

Figure 6. Comparison of (a) the current monitored on the NDCX internal electrodes with bias voltages set to clear electrons, and (b) the corresponding WARP calculation.

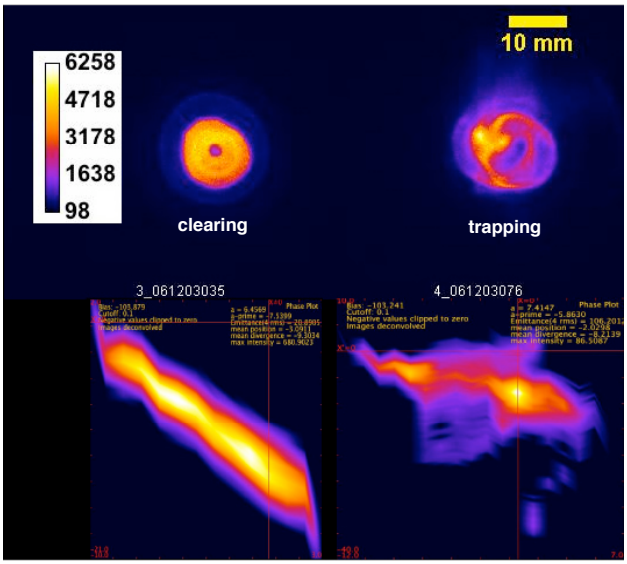

Figure 7. Left column: measured transverse beam distribution; right column: measured transverse phase space (note scale difference) for the clearing case and the trapping case.

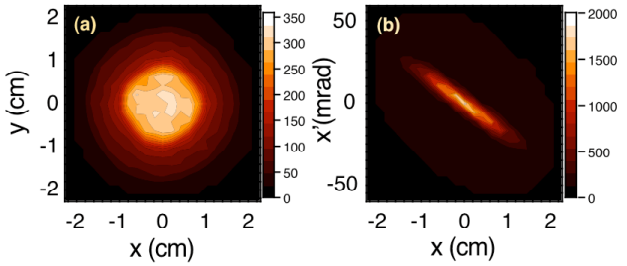

Figure 8. WARP simulations of the beam (a) transverse structure and (b) phase space for a case where the bias pattern of internal electrodes is chosen to clear electrons. This image is a projection of the final 0.5 m of beam, recorded 4 μs into the pulse.

Table 1: Measured and simulated beam envelope radius a, and envelope angle a', for electrostatic quadrupoles, magnetic quadrupoles, and magnetic solenoids. Both X and Y values are given for magnetic quadrupoles only.

	Electrostatic Quads		**Magnetic quads**		**Magnetic quads**		**Sol. Magnets**	
	a (mm)	**a' (mrad)**	**a (mm)**	**a' (mrad)**	**b (mm)**	**b' (mrad)**	**a (mm)**	**a' (mrad)**
Experiment	12.24	38.52	12.0	-18.8	18.4	31.6	7.37	-11.04
Simulation	12.07	35.46	14.42	-14.39	18.28	33.82	8.10	-10.20

experimental current grows to about 50 mA. The experimental waveform is used in the simulations, so that is accurate; however, either the mesh size or the time step may be too large near the ion-emitting surface in the source. These possibilities are being checked.

Images of the transverse beam structure, like those in Fig. 7 taken about 5 μs into pulse with a 500-ns gate, show a clear difference between the clearing and trapping bias patterns. The co-ordinate space image for the clearing pattern shows a roughly circular 6.3-cm beam spot, with the density varying by about 25 % across the top plus a small 50% density depression at the center. The transverse phase space for this case shows the beam emittance of 19 mm-mrad and an envelope convergence angle of -8.5 mrad. In contrast, the case with the bias set to trap electrons has a larger spot size, a very irregular density profile, and an emittance that is five times larger than is found for the other bias pattern.

We estimate the electron density from the currents to the electrodes. For the clearing bias case, we set the electron energy to the electrode bias to determine the electron velocity; then from the continuity equation we compute an electron line charge of 0.5% of the beam line charge. For the trapping bias, we assume that all emitted electrons are trapped; integrating the emission current yields an electron line charge of ~80% of the beam line charge. These values should be regarded as preliminary, as they have not been critiqued and cross-checked to the degree that our measurements of electron line charge in quadrupoles have been verified [13].

Simulations of clearing cases provide reasonable agreement with experimental data, showing an approximately circular spot and uniform convergence angle. Fig. 8, for example, shows a projection of the final meter of beam at 4 μs. Unlike the experiment, however, cases with electrode voltages chosen to trap electrons show nearly the same transverse structure and time history. This result is not surprising. We currently believe that we have beam halo that scrapes the electrodes, producing electron and gas emission from the surfaces. We measure emission currents from negatively biased electrodes that are consistent with this hypothesis. However, beam halo has been observed to be significantly worse, even in experiments designed to minimize and study halo [38], than it is in simulations, and circumstantial evidence indicates that the same is true in our experiments and simulations. Without a mechanism to generate the observed gap-electrode current in the trapping case, the simulations will not be able to reproduce the trapped electron density or the effects of this on the beam emittance.

We have compared measured and computed beam envelopes for electrostatic quadrupole transport [30], magnetic quadrupole transport [39] and solenoid transport of heavy-ion beams [32], for cases where e-clouds are minimized. (Note that e-clouds are expected to be absent with electrostatic quadrupoles for which the applied electric field dominates over the space-charge field of the beam.) We find agreement in the radius (a) to within 10% or 1 mm and envelope angle (a') to within 10% or 3 mrad in these cases, as listed in Table 1; except that for magnetic quadrupoles the error was as large as 23% in the X envelope angle but only 7% in the Y angle, and 0.7% in the Y radius. The agreement between experiment and simulation is similar to the accuracy of the experimental data. Each case was evaluated carefully, but with slightly different techniques, which we plan to discuss in more detail in a future publication.

From this agreement, we conclude that theoretical estimates of beam-current limits are accurate, as long as e-clouds are small enough to have a negligible effect on the beam. Other results in this paper demonstrate that clearing and suppression electrodes are effective at minimizing e-cloud densities to such negligible levels.

ACKNOWLEDGEMENTS

We are grateful to B. Grant Logan for his support and to Matthaeus Leitner, Will Waldron, Wayne Greenway, Ralph Hipple, William Strelo, Tak Katayanagi, Eugene Flor, Cory Lee, Michael Dickinson, Gary Ritchie, David Baca, Craig Rogers, and Ed Romero for excellent technical support. This work was performed under the auspices of the U.S. Department of Energy by University of California, Lawrence Livermore National Laboratory under contract No. W-7405-Eng-48, and by University of California, Lawrence Berkeley National Laboratory under Contract DE-AC03-76F00098.

REFERENCES

[1] Proceedings of the E-Cloud'02 and E-Cloud'04: http://wwwslap.cern.ch/collective/ecloud02/proceedings/index.html and http://mafurman.lbl.gov/ECLOUD04_proceedings/

[2] S. Y. Zhang, "ICFA Workshop on Beam Induced Pressure Rise in Rings," http://www.c-ad.bnl.gov/icfa (2003).

[3] B. G. Logan et al., Nucl. Fusion **45**, 131 (2005).

[4] R. Davidson et al., "Frontiers in High Energy Density Physics: The X-Games of Contemporary Science," The National Academies Press (2003).

[5] N. A. Tahir et al., Phys. Rev. Lett. **95**, 035001 (2005).

[6] R. H. Cohen, A. Friedman, S. Lund, A. W. Molvik, E. P. Lee, T. Azevedo, J.-L. Vay, P. Stoltz, and S. Veitzer, "Electron-Cloud Simulation and Theory for High-Current Heavy-Ion Beams," Physical Review Special Topics – Accelerators and Beams **7**, 124201 (2004).

[7] A. W. Molvik, M. Kireeff Covo, F. M. Bieniosek, L. Prost, P. A. Seidl, D. Baca, A. Coorey, and A. Sakumi, "Gas desorption and electron emission from 1 MeV potassium ion bombardment of stainless steel," Physical Review Special Topics – Accelerators and Beams **7**, 093202 (2004b).

[8] J.-L. Vay, P. Colella, J. W. Kwan, et al, Phys. Plasmas 11, 2928 (2004).

[9] J.-L. Vay, M. A. Furman, P. A. Seidl, LBNL, R. H. Cohen, A. Friedman, D. P. Grote, M. Kireeff Covo, A. W. Molvik, LLNL, P. H. Stoltz, S. Veitzer, Tech-X Corp., J. Verboncoeur, UC Berkeley, Proceedings of the 2005 Particle Accelerator Conference, Knoxville, TN, May 16-20, 2005 (IEEE, Piscataway, NJ, 2003) p. 525.

[10] A. W. Molvik, M. Kireeff Covo, A. Friedman, R. Cohen, S.M. Lund, J.J. Barnard, LLNL,; F. Bieniosek, P. Seidl, D. Baca, J.-L. Vay, C.M. Celata, W.L. Waldron, LBNL, ; J.L. Vujic, Univ. California, Berkeley, "Experiments Studying Desorbed Gas and Electron Clouds in Ion Accelerators," Invited paper at 2005 Particle Accelerator Conference, Knoxville, TN, May 16-20, 2005. Proceedings of 2005 Particle Accelerator Conf., Knoxville, TN., IEEE (2005), p. 194.

[11] R. H. Cohen, A. Friedman, M. Kireeff Covo, S. M. Lund, and A. W. Molvik, F. M. Bieniosek, P. A. Seidl, J.-L. Vay, P. Stoltz and S. Veitzer, "Simulating electron clouds in heavy-ion accelerators," Invited paper at APS-DPP, Savannah, Nov. 2004, Phys. Plasmas **12**, 056708 (2005).

[12] M. Kireeff Covo; Molvik, A.W.; Friedman, A.; Westenskow, G.; Barnard, J.J.; Cohen, R.; Seidl, P.A.; Kwan, J.W.; Logan, B.G.; Baca, D.; Bieniosek, F.M.; Celata, C.M.; Vay, J-L.; Vijic, J.L., "Beam Energy Scaling of Ion-Induced Electron Yield from K+ Impact on Stainless Steel", Physical Review Special Topics **9**, 063201 (2006).

[13] M. Kireeff Covo, Molvik, A.W.; Friedman, A.; Vay, J-L.; Seidl, P.A.; Logan, B.G.; Baca, D.; Vujic, J.L., "Absolute Measurement of Electron Cloud Density in a Positively-Charged Particle Beam", Physical Review Letters **97**, 054801 (2006).

[14] R. H. Cohen, A. Friedman, D. P. Grote, J.-L. Vay, "Large-timestep mover for particle simulations of arbitrarily magnetized species," Submitted to Nucl. Instrum. Methods A. (2007).

[15] M. Kireeff Covo; Molvik, A.; Friedman, A.; Barnard, J.J.; Seidl, P.A; Logan, B.G.; Baca, D.; Vujic, J.L., "Beam Interaction Measurements with a Retarding Field Analyzer", Nuclear Instruments and Methods in Physics Research A **577**, 139 (2007).

[16] A.W. Molvik, Kireeff Covo, M.; Cohen, R.H.; Friedman, A.; Bieniosek, F.M.; Seidl, P.A.; Vay, J-L., "Quantitative electron and gas cloud experiments", Nucl. Instrum. Methods **A 577**, 45-51 (2007).

[17] A.W. Molvik, H. Kollmus, E. Mahner, M. Kireeff Covo, M. C. Bellachioma, M. Bender, F. M. Bieniosek, E. Hedlund, A. Krämer, J. Kwan, O. B. Malyshev, L. Prost, P. A. Seidl, G. Westenskow, L. Westerberg, "Heavy-ion induced electronic desorption of gas from metals," Phys. Rev. Lett. **98**, 064801, (2007).

[18] A.W. Molvik, J-L. Vay, M. Kireeff Covo, R. Cohen, D. Baca, F. Bieniosek, A. Friedman, C. Leister, S. M. Lund, P. Seidl, and W. Sharp. "Quantitative experiments with electrons in a positively charged Beam," Phys. Plasmas **14**, 056701 (2007).

[19] J.-L. Vay, "Noninvariance of space- and time-scale ranges under a Lorentz transformation and the implications for the study of relativistic interactions," Phys. Rev. Lett. 98, 130405 (2007).

[20] J.-L. Vay, M. A. Furman, P. A. Seidl, *et al*., "Self-consistent simulations of heavy-ion beams interacting with electron-clouds," Nucl. Instrum. Methods A **577**, 65 (2007).

[21] M. Plum, J. Allen, M. Borden, D. Fitzgerald, R. Macek, T. S. Wang, Proc. Of the Particle Accelerator Conference, p. XXX (IEEE, ????).

[22] E. Jones, F. Pedersen, A. Poncet, S. van der Meer, E. J. N. Wilson, IEEE Transactions on Nucl. Sci. NS-32, 2218 (1985).

[23] T. Kasuga, Japanese J. of App. Phys. 25, 1711 (1986).

[24] Y. Miyahara, J. Vac. Sci. Technol. A **5**, 2927 (1987).

[25] F. Pedersen, A. Poncet, L. Soby, Proc. Of the 1989 Particle Accelerator Conference, (IEEE, 1989).

[26] H. Halama, E. Bozoki, Proc. Of the 1991 Particle Accelerator Conference, p. 2313 (IEEE, 1991).

[27] E. V. Bulyak, Proc. Of the 1993 Particle Accelerator Conference, p. 3512 (IEEE, 1993).

[28] K. Emura, T. Shinzato, H. Takada, Nuc. Instr. And Meth. In Phys. Res. A 419, 45 (1998).

[29] X. Q. Wang, Y. J. Pei, X. L. Dong, H. L. Xu, L. Shang, L. Wang, K. J. Fan, G. C. Wang, C. G. Yao, S. M. Hu, X. F. Luo, Proc. Of the 1999 Particle Accelerator Conference, p. 1596 (IEEE, 1999).
[30] L. R. Prost et al., Phys. Rev. ST AB 8, 020101 (2005).
[31] P. Roy et al, Phys. Rev. Lett. 95, 234801 (2005).
[32] J. E. Coleman, et al., "Electron cloud effects on an intense ion beam in a four solenoid lattice," to be submitted to PRSTAB.
[33] M. Tobiyama, J. W. Flanagan, H. Fukuma, S. Kurokawa, K. Ohmi, and S. S. Win, "Coupled bunch instability caused by an electron cloud," PRSTAB 9, 012801 (2006).
[34] D. P. Grote, A. Friedman, I. Haber, Fus. Eng. & Des. 32-33, 193 (1996), available at http://hif.lbl.gov/theory/WARP.summary.html
[35] D. P. Grote, A. Friedman, I. Haber, W. M. Fawley, and J.-L. Vay, Nucl. Instrum. Methods Phys. Res. A 415, 428 (1998).
[36] M. A. Furman and M. Pivi, Phys. Rev. ST Accel. Beams 5, 124404 (2002).
[37] See http://www.txcorp.com/technologies/TxPhysics/.
[38] C. K. Allen, K. C. D. Chan, P. L. Colestock, K. R. Crandall, et al., "Beam-halo measurements in high-current proton beams, Phys. Rev. Lett. 89, 214802 (2002).
[39] P. A. Seidl, et al., APS Div. Of Plasma Physics, Denver, Oct. 2005, paper BP1-90.

.